Mechanical Engineering Research; Vol. 10, No. 1; 2022
ISSN 1927-0607 E-ISSN 1927-0615
Published by Canadian Center of Science and Education

Modeling of a Zero CO_2 and Zero Heat Pollution Compressed Air Engine for the Urban Transport Sector

Ngang Tangie Fru[1], Nébo K. Yohan Arnold[1], Biyéné Florent[1], Kom K Yvan Armel[1], Kanmogne Abraham[1] & Ngoumkoua Wamba Chamberlin[1]

[1] Department of Mechanical Engineering, National Advanced School of Engineering (ENSP), University of Yaounde 1, Cameroon

Correspondence: Ngang Tangie Fru, Department of Mechanical Engineering, National Advanced School of Engineering (ENSP), University of Yaounde 1, Cameroon. E-mail: ngang313@yahoo.com

Received: October 26, 2021 Accepted: December 15, 2021 Online Published: December 26, 2022

doi:10.5539/mer.v10n1p25 URL: https://doi.org/10.5539/mer.v10n1p25

Abstract

Zero CO2 and Zero heat pollution compressed air engine for the urban transport sector is an engine design that is powered and lubricated solely by compressed air. In other to guarantee these functionalities for the engine design, its modeling was done following the mechanical engineering design method. This article highlights the creation of a mathematical model of the engine. This work covers the design synthesis and the analysis of the kinematics of the engine. For the design synthesis; FAST, GRAFCET and later one realization of conceptual sketches all deductions from the problem definition. With the sketches considered, the kinematics and dynamic formulations where later on realized. The design chosen highlight's the external forces to come principally from an isothermal expansion process of the compressed air what is termed the expansion chamber of the engine. The analysis was done on the kinematics of the engine with considerations of some assumptions. This article ends with remarkable results as it concerns the engine's simplicity and guaranteed high efficiency. These conclusions were drawn from the compact nature of the design, the low part count and the reduced displaceable masses which give little of no conflicting movements in the engine design.

Keywords: compressed air engine, kinematics, dynamics, model, isothermal expansion

1. Introduction

When the natural balance of ozone destruction and production is altered more towards destruction, the term "ozone depletion" is christened (Angell & Korshover, 2005). The gases that cause a rapid depletion of the ozone layer equally fall under the greenhouse gases category (Sivasakthivel & Siva, 2011). Greenhouse gases are the main contributors of global warming. These gases consisting of mainly carbon oxides, methane and CFCs, accumulated in the troposphere (8 to 16 km in the atmosphere) (Fergusson, 2001). This research work introduces us to a new area of study in the fight against heat and air pollution as it contributes to establishing a mathematical model for a zero CO2, Zero Heat Pollution Compressed Air Engine for the urban transport sector.

A compressed air engine consists of a motor that is powered and lubricated solely on compressed air (Rathod & Arvind, 2012). Compressed Air Engine technology has proven its feasibility over centuries as its designs have moved from pneumatic engines, pneumatic heated engines to compressed air engines. Dennis Papin first spoke of such an engine in 1687, but it was not until 1872, that the Mekarski invented an air engine that functioned as Papin had earlier mentioned (Verma, 2008). In 1892, another heating method was introduced by Robert Hardie to improve on the range of the engine (Rathod & Arvind, 2012). In 1898, Hoadley and Knight, made the first urban locomotive based on the principle that the longer the air is kept in the engine the more heat it absorbed and the greater will be its range. As a result, they introduced a two-stage engine (Thipse, Compressed Air Car, 2008). Engineair Pty Ltd of Australia and Moteur Development International of France are some of the few companies nowadays that hold the international patents for the compressed air engines designs (Verma, 2008).

The zero CO_2 and zero heat pollution compressed air engine principally adapted for the cities in the Tropics will be a significant step towards generating contextualized solutions to this climate change calamity. This research work is not just all about terminating the use of other energy forms in the transport sector but it is about assuring their more sustainable use. This article demonstrates how an appropriate compressed air engine model is created. This model takes into consideration kinematic and dynamic needs of the engine and also the attributes of the

tropical environment for which the engine is essentially designed for.

2. Method and Materials

To come out with a model of a compressed air engine, this article covered two stages of mechanical engineering design; design syntheses and analysis. The synthesis follows the definition of the problem which does not fall within the scope of this article. Under the synthesis; the functional analysis (FAST), automation of the engine (GRAFCET), development of structural sketches, kinematic and dynamic formulations. The analysis stage covers the MatLab simulations of these formulas and discussions of the end results.

3. Design Synthesis

3.1 Functional Analysis Structure Technique (FAST)

From the FAST display was extracted the following key components that play a major role in the functioning of the compressed air engine;

1. A reusable insulated compressed air storage cylinder (SC).
2. A multivariable transmitter for measurement (MT).
3. Throttle like valve (TV).
4. High pressure good heat conduction metallic pipe network (MP).
5. Adjustable metallic slot timer (ST) with inject slot (IS) and exhaust slot (ES).
6. Quasi fixed volume reception chamber (RC), equally called the pre expansion chamber; enclosed by the slot timer and a lid.
7. Enclosed poor heat conduction stator or casing, hexagonal cross section.
8. Poor conduction inlet manifold (IM) separate routes, some leading to EC (Primary Passages (PP)), while others the inner surface of the rotor (Secondary Passages (SP)).
9. Light metallic wings.
10. Dense metallic fixed axial rotor assembly.
11. The wings together with the inner walls of the stator and outer walls of the rotor enclose the expansion chamber (EC).
12. Exhaust manifold and stator lid (EM).

3.2 Automation of Compressed Air Engine Operation

Bearing in mind the “independent function”, “self”, “Maxwell and Reciprocity” and “symmetry” principles of mechanical design; an automated process model of the operation of this engine was derived using the GRAFCET technique.

Given this engine design is expected to operate mechanically and parts count reduced to a minimum, the sensors used in its operation will be reduced to one that is the multivariable transmitter. The operation is expected to be continuous with momentary interventions done by the operator. The main source of power being the compressed air stored in the cylinder.

The operation process of this engine is momentarily initiated with the opening of the stop-cup which is then followed by an iterative process of running and adjustment of the engine with pulsated operator intervention or not for an economic running of the engine. This study permits the establishment of a compact design of the engine.

3.3 Structural Conceptual Sketches of the Compressed Air Engine

With a close appreciation of mechanical design principles like; “Saint-Venart’s” principle, “Symmetry” Principle, “Triangulate for Stiffness” Principle, “Maxwell and Reciprocity” principle, “Stability” principle, “Avoid Bending Stresses” Principle, “Manage Friction” Principle, and “Self-Principles” (Craig, 2011), an understanding of the functioning and automation of the engine, next step was the conceptual structural sketches of the main component parts of the engine and their assembly. These figures were drawn using the Golden Rectangle Rule dimensional principles (Craig, 2011). The end result of this study is a compact engine assembly with tentative dimensions as depicted in figure 1 below.

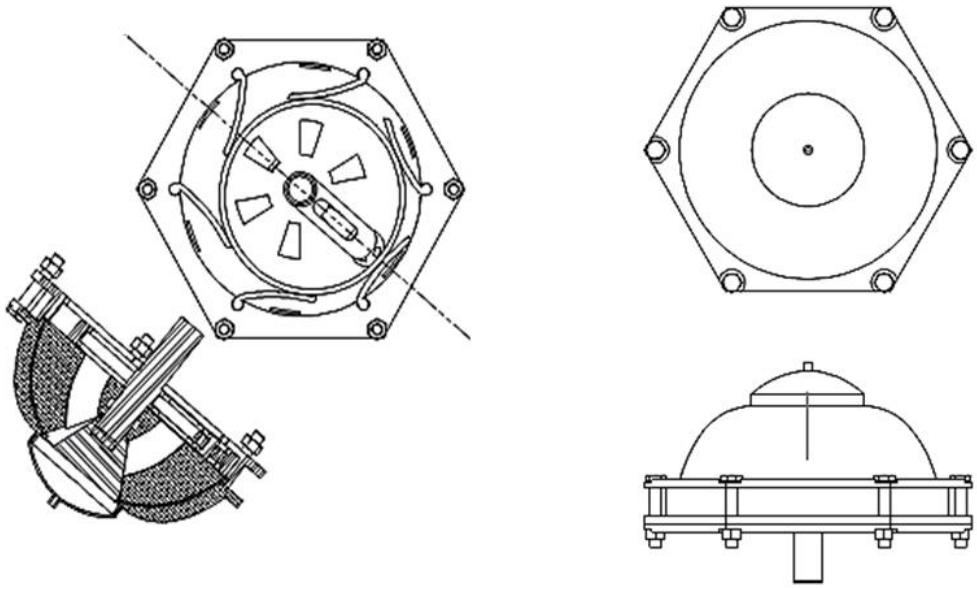

Figure 1. Engine assembly

3.4 Kinematic Formulation of the Engine

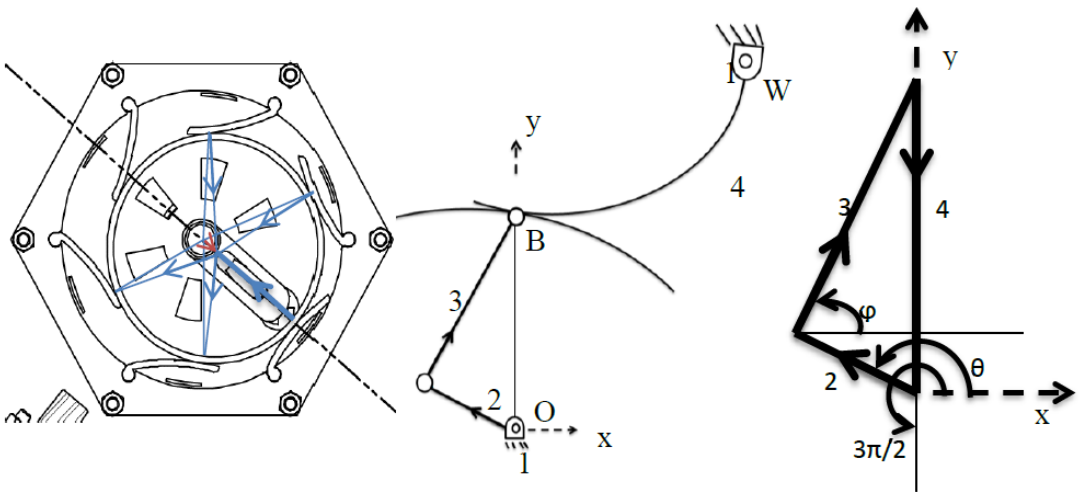

Figure 2. Engine skeleton diagram

After identifying the moving components of the engine, a skeleton of the engine was constructed and then the kinematic formulation of the engine deduced as per the variables associated to the skeleton diagram presented above in figure 2.

In an attempt to reduce the number of unknowns, the following qualities were used to determine three of the unknowns;

- θ varies continuously in the interval $[0,2\pi]$, thus is considered known,
- r_2 is a positive constant and its magnitude is equal to the maximum linear, displacement of the wing from the walls of the stator,
- r_3 is a positive constant. It has a steady ratio with r_2 it is assumed that they are related as follows;

$$\frac{r_2 + r_3}{r_3} \leq 1.618 => r_2 \leq 0.618 r_3$$

Thus the following position functions were then deduced for the other unknowns;

$$r_4 = r_2 \sin\theta + \sqrt{{r_3}^2 - {r_2}^2 \cos^2\theta} \quad (1)$$

$$\varphi = \tan^{-1}\left[\frac{\sqrt{{r_3}^2 - {r_2}^2 \cos^2\theta}}{r_2 \cos\theta}\right] \quad (2)$$

Assuming that;

- r_2 is a constant with respect to time,
- r_3 is a constant with respect to time,
- $\dot{\theta} = \omega$ is considered known as it represents the output angular velocity of the engine.

The following velocity functions deduced

$$\dot{\varphi} = \frac{-r_2 \omega \sin\theta}{r_3 \sin\varphi} \quad (3)$$

$$\dot{r_4} = \frac{r_2 \omega \sin(\varphi - \theta)}{\sin\varphi} \quad (4)$$

With an assumption on knowledge of the angular acceleration (α) of the engine, the following acceleration functions deduced

$$\ddot{\varphi} = \frac{r_3 \dot{\varphi}^2 \cos\varphi + r_2 \omega^2 \cos\theta + r_2 \alpha \sin\theta}{-r_3 \sin\varphi} \quad (5)$$

$$\ddot{r_4} = \frac{r_3 \dot{\varphi}^2 + r_2 \omega^2 \cos(\varphi - \theta) - r_2 \alpha \sin(\varphi - \theta)}{-\sin\varphi} \quad (6)$$

3.5 Dynamics Formulations of Engine

The formulation of the engine's dynamics is by using the inverse dynamics. It is assumed here that the principal external force is that which results from the thermodynamic expansion and with a mastery of the kinetics of the engine, the internal forces were formulated so as to guarantee the kinematics of this engine.

It was from the understanding of the dynamics formulations that dimensional estimates of parameters like the required displacements of the wings (r_2) and then (r_3) are gotten. This calculation starts with the thermodynamic formulations of the external forces followed by the balancing of internal and external forces of the system.

3.5.1 Thermodynamic Formulation

This conversion actually involves two thermodynamics processes, first a reversible expansion process in the reception chamber, then an irreversible expansion in the expansion chamber.

Reversible expansion

The reversible expansion takes place at the reception chamber and involves a reversible change of the pressure, volume and temperature. The reversible expansion process consists of an isothermal injection, adiabatic expansion, isochoric compression and isobaric exhaust through the slots of the slot timer as can be seen in figure 3 below.

Suppose the following assumptions;

- P_1: the pressure of the compressed air from the cylinder which is known.
- T_1: the temperature of the compressed air from the cylinder, which is known.
- V_1: the volume of the compressed air at P_1 and T_1 injected into the RC, which is unknown.
- P_2: the pressure of the compressed air after an isothermal expansion, which is unknown.
- T_2: the temperature of the compressed air after an isothermal expansion, which is known to be T_1.
- V_2: the volume of the RC, which is known.
- P_3: the pressure of the compressed air after an isochoric compression, which is known to be P_1.
- T_3: the temperature of the compressed air after an isochoric compression, which is known to be the room temperature $(25℃)$.
- V_3: the volume of the RC, which is known.

The isobaric exhaust falls on line with the isothermal injection and as a result, the following assumptions are

made;

- P_4: the pressure of the compressed air during an isobaric exhaust, which is known to be P_1.
- T_4: the temperature of the compressed air during an isobaric exhaust, which is known to be the room temperature.
- $\dot{V}_4$: the volumetric flow rate of the compressed air during an isobaric exhaust, which is known.
- MM_{air} is the molar mass of air and ρ its density.

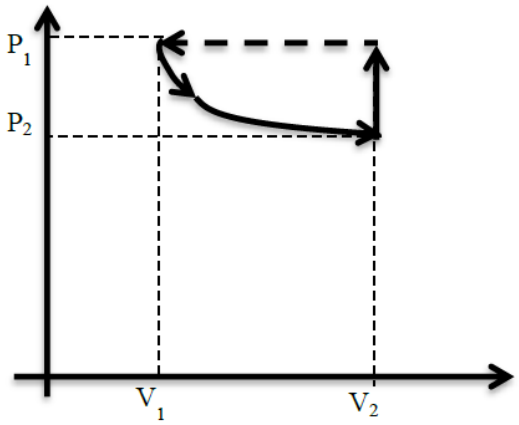

Figure 3. PV- curve of the adiabatic expansion process

The following equations are thus deduced

$$P_2 = \frac{\rho R T_1}{MM_{air}} \tag{7}$$

$$V_1 = \frac{P_2 V_2}{P_1} \tag{8}$$

$$P_3 = \frac{P_2 T_3}{T_2} \tag{9}$$

Assuming that a more significant energy gain is witnessed during the isochoric expansion process, this energy gain is considered equivalent to the internal energy added to the system and so is expressed as;

$$\Delta U = c_v(T_3 - T_2) \tag{10}$$

Isothermal expansion

The isothermal expansion is an irreversible process. This involves a very significant change in the volume and pressure. The isothermal expansion process consists of an isobaric injection, isothermal expansion and then an isobaric exhaust as shown in figure 4 below.

The following assumptions are essential for a proper formulation of this process.

- P_5: the pressure of the compressed air after the isobaric injection, which is known as P_4.
- T_5: the temperature of the air after the isobaric injection, which is known as T_4.
- V_5: the volume of the compressed air after the isobaric injection, which is known as $V_5 = V_2$.
- P_6: the pressure of the decompressed air after an isothermal expansion, which is known as atmospheric pressure $+1000\ Pa\ max$.
- T_6: the temperature of the decompressed air after an isothermal expansion, which is known as T_5.
- V_6: the volume of the decompressed air, which is unknown.
- W_{wi}: work done by a single wing
- After the isobaric exhaust, the air left in the EC is assumed to be at room temperature and pressure.

It should be noted that the dotted line represents almost instantaneous isochoric compression which occurs with

the turbulence that is created as very high-pressure fluid rushes through the inlet of the EC.

- From understandings on the isobaric injection process and the assumption that the temperature of the compressed air is constant, the injection here is seen to have no significant thermodynamic change.

From understandings on this isothermal expansion process, the following was deduced.

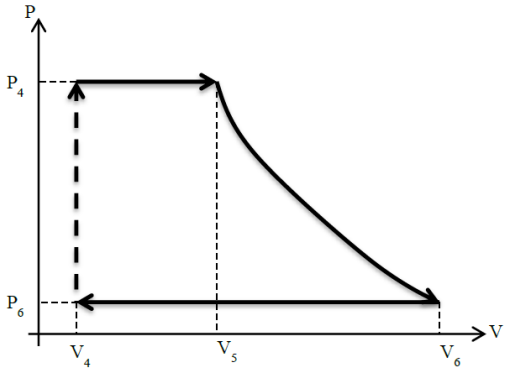

Figure 4. Irreversible expansion process

$$V_6 = \frac{P_5 V_5}{P_6} \tag{11}$$

$$V_5 = \frac{r_2 f_1 \sin\theta}{P_5 \ln\frac{P_5}{P_6}} \tag{12}$$

$$W_{wi} = P_5 V_5 \ln\frac{V_5}{V_6} \tag{13}$$

3.5.2 Establishment of Relationships between the Internal and External Forces

Consider the free body diagram in figure 5 below;

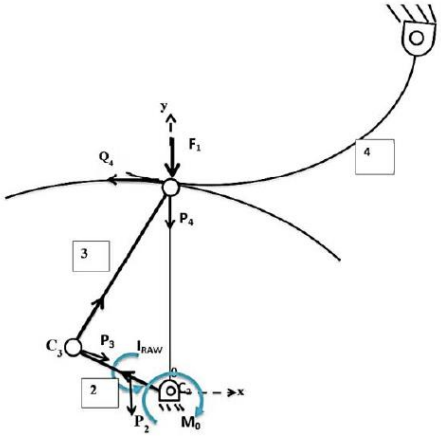

Figure 5. Vector representation of dynamic forces of the engine

While P_i are the internal forces of the different moving objects, F_i are the useful/exploitable forces and Q_4 is the frictional force that keeps the wings steadily attached to the rotor cylinder. The corresponding small letters are the magnitudes of these forces. From D'Alembert's principal and other deductions done, we see that;

$$f_{34}{}^{\varepsilon} = f_1 - p_4 \tag{14}$$

For

$$\zeta_3 = M_3{}^{i} + p_3 r_3 \cos(\theta - \varphi) \tag{15}$$

$$\zeta_4 = r_3(q_4 \sin^2\varphi + \zeta_1 \sin\varphi + p_3 \cos\varphi \sin(\theta - \varphi)) \tag{16}$$

$$=> r_2 = \frac{\zeta_2\left(M_0 + M_2^i - p_2 r_{RAW}\right)}{p_3\zeta_2 + \zeta_3(\cos\varphi + \sin\varphi\tan\theta) + \zeta_4(\tan\varphi - \tan\theta)} \tag{17}$$

Where;

- $M_3{}^i = I_{cyl}\alpha(0,0,1)^T$
- $M_2^i = I_{RAW}\alpha(0,0,1)^T$
- $I_{cyl}, I_{RAW}\ and\ r_{RAW}$ were deduced to be;
  - $I_{cyl} = m_{cyl}{r_3}^2$
  - $I_{RAW} = the\ moment\ of\ inertia\ of\ the\ rotor\ arm - wheel\ assembly$ and
  - r_{RAW} $= distance\ from\ centre\ of\ rotation\ of\ rotor\ to\ center\ of\ mass\ of\ RAW(rotor\ and\ rotor\ wheel\ assembly)$

4. Result and Discussion

With the use of MatLab, the following analysis were done, displayed graphically with references to the formulae.

4.1 Position Vector Analysis

Studies here are carried out on $r_4(\theta)$ and $\varphi(\theta)$ with r_2 considered to vary discretely from 5cm.

Dependent variables	Source
$\boldsymbol{r_4(\theta)}$	(-1)
$\boldsymbol{\varphi(\theta)}$	(-2)

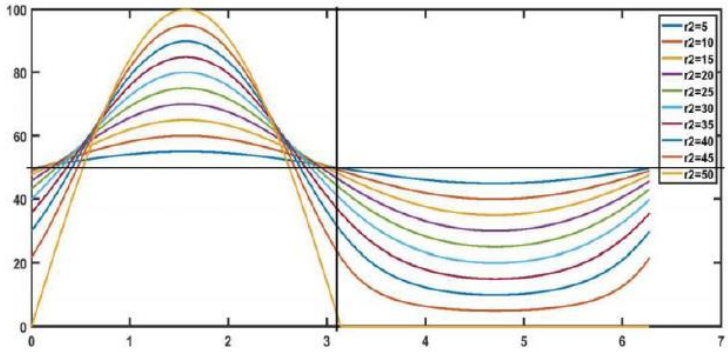

Figure 6. Variation of $\boldsymbol{r_4}$ w.r.t $\boldsymbol{\theta}$

The graph above (figure 6) is a plot of the contact point position of one of the wings to the rotor cylinder with the rotor undergoing an anticlockwise rotation$[0,2\pi]$ from the x−axis. It is also seen that this study was carried out for varying lengths of the distance between the centre of the cylinder and the supposed centre of its revolution which is a radius equivalent to the maximum displacement of the furthest portion of the wings from the stator. In this graph, can be seen that the positioning of the contact point at the start is midway then it rises to its maximum position which implies the wing is closest to the stator, back to midway and further to the minimum position (furthest displacement of the wing from the stator) and again back to midway. The needed repetitive nature of this displacement is assured in this kinematic study with room is given for a quick expansion of the compressed air and its exhaust making sure the exhaust effort is reduced. The variations in the timing of the supposed perfect intake, expansion and exhaust moments can be seen for the various curves for varying r_2; thus, the best fit $r_2{:}r_3$ proportions could be deduced.

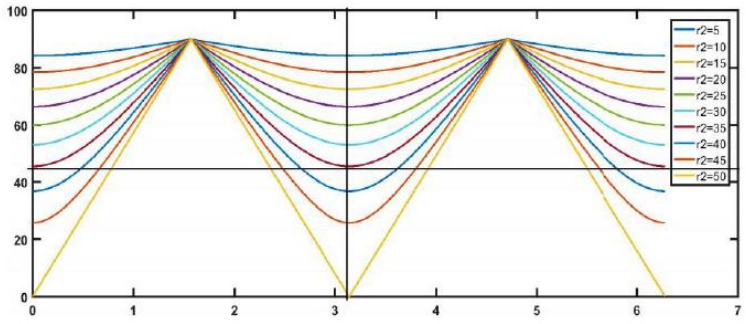

Figure 7. Variation of $\boldsymbol{\varphi}$ w.r.t. $\boldsymbol{\theta}$

This graph (figure 7) further indicates that at $\theta = \pi/2, \varphi = 90°$ and at $\theta = 3\pi/2, \varphi = 90°$ implying points of inflection thus there is room for the injection and exhaust at these respective points.

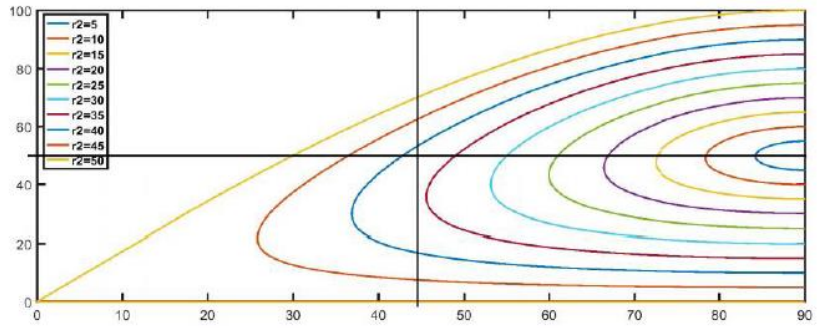

Figure 8. Variation of $\boldsymbol{r_4}$ w.r.t. $\boldsymbol{\varphi}$

The single closed loop displayed above (figure 8) for each of the values of r_2 is a clear indication of the absence of any conflicting displacement in the design of this engine; a clear indication of the absence of conflicting position vectors.

4.2 Velocity Analysis

Studies here are carried out on $\dot{r_4}(\theta, \omega, \varphi)$ and $\dot{\varphi}(\theta, \omega, \varphi)$.

Dependent variables	Source
$\boldsymbol{\dot{r_4}(\theta, \omega, \varphi)}$	(-3)
$\boldsymbol{\dot{\varphi}(\theta, \omega, \varphi)}$	(-4)

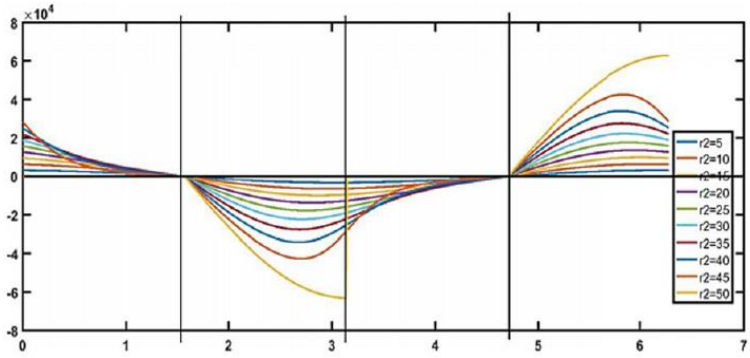

Figure 9. Variation of the linear velocity $\boldsymbol{\dot{r_4}}$ w.r.t. $\boldsymbol{\theta}$

Momentary stagnation in the displacement of the wings can be observed at $\theta = \pi/2 \; and \; 3\pi/2$ (figure 9); this happens to be just when the wing is furthest from the rotor's centre of rotation and when it is closest. These stagnations give room for an injection and exhaust free from conflicting movements thus an optimal use of energy.

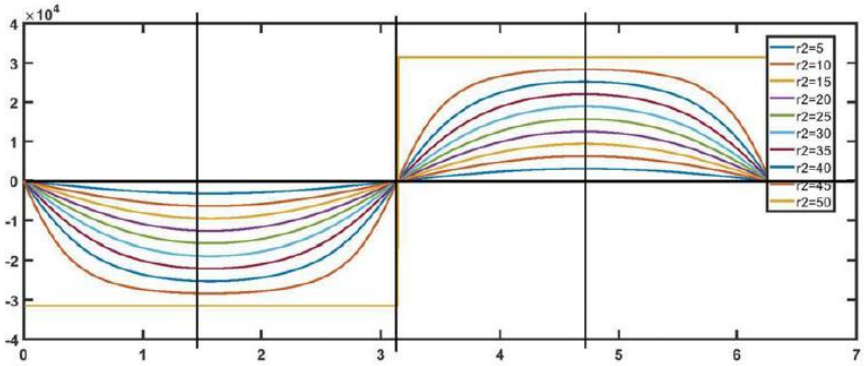

Figure 10. Variation of the angular velocity $\boldsymbol{\dot{\varphi}}$ w.r.t. $\boldsymbol{\theta}$

$\dot{\varphi}$ is the speed of revolution of the rotor cylinder about the centre of rotation. The graph above (figure 10) indicates the absolute value of this angular speed is maximum when the linear motion at the wing is supposedly stagnant. This indicates how swift the change from a supposedly linear stagnation at the wings will be thus assuring the continuity of motion of the system.

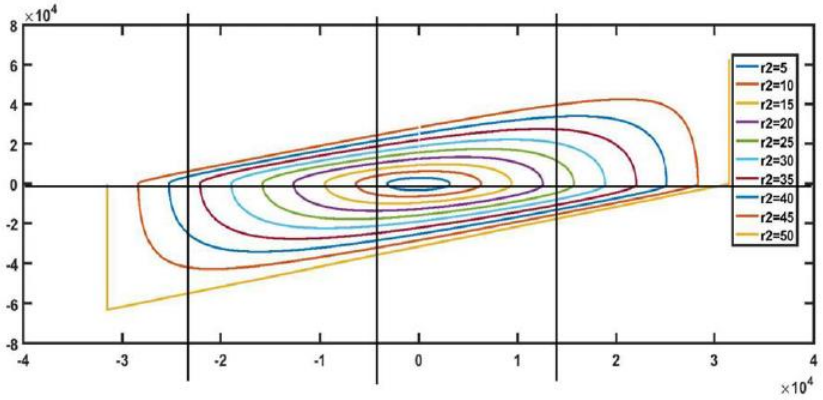

Figure 11. Variation of the linear velocity $\dot{\boldsymbol{r}}_{\boldsymbol{4}}$ w.r.t. $\dot{\boldsymbol{\varphi}}$

The graph above (figure 11) shows two symmetric loops that are reflective about the x-axis and these loops meet at the point $(0,0)$ which further indicates the smoothness displacement rate of the engine movable components.

4.3 Acceleration Analysis

Studies here are carried out on $\ddot{r}_4(\alpha, \omega, \theta, \varphi, \dot{\varphi})$ and $\ddot{\varphi}(\alpha, \omega, \theta, \varphi, \dot{\varphi})$.

Dependent variables	Source
$\ddot{\boldsymbol{r}}_{\boldsymbol{4}}(\boldsymbol{\alpha}, \boldsymbol{\omega}, \boldsymbol{\theta}, \boldsymbol{\varphi}, \dot{\boldsymbol{\varphi}})$	(-5)
$\ddot{\boldsymbol{\varphi}}(\boldsymbol{\alpha}, \boldsymbol{\omega}, \boldsymbol{\theta}, \boldsymbol{\varphi}, \dot{\boldsymbol{\varphi}})$	(-6)

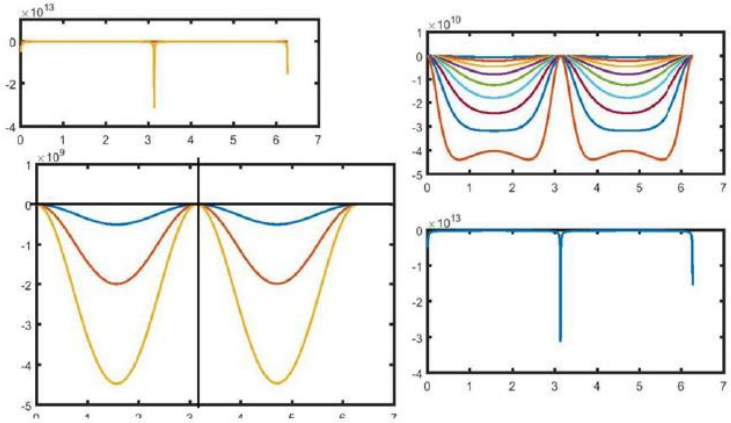

Figure 12. Variation of the acceleration $\ddot{\boldsymbol{r}}_{\boldsymbol{4}}$ w.r.t. $\boldsymbol{\theta}$

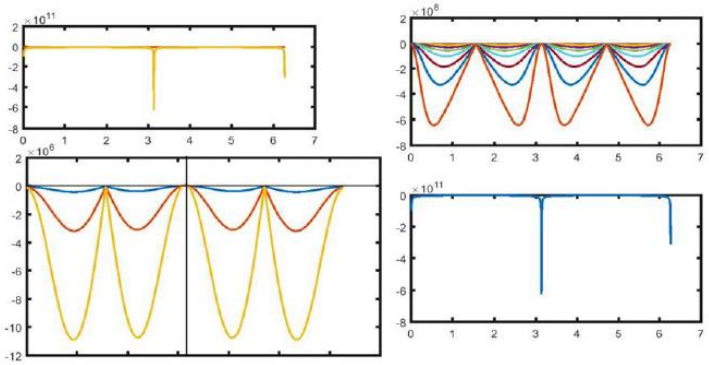

Figure 13. Variation of the angular acceleration $\ddot{\varphi}$ w.r.t. θ

Considering the great disparities in the plots for vary r_2, there was some separations in the graphs for better visibility (figure 13). In the plots for which r_2 was taken to vary from 5 to 15, one could clearly see that the linear acceleration of the wing corresponds with the areas of stagnation which is a clear indication of the continuity of displacement that is achieved with the setup. This is not the case as r_2 gets closer to 50cm. In the later, the symmetry starts becoming questioned with a complete offset at $r_2 = 50cm$.

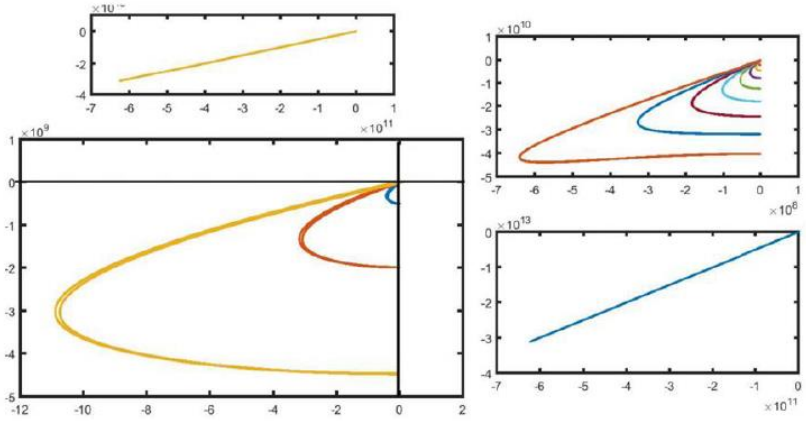

Figure 14. Variation of the acceleration $\ddot{r}_4$ w.r.t. $\ddot{\varphi}$

In the figure above (figure 14) is observed the repetitive nature of the displacement pattern of this engine with almost zero changes for the return loop. This necessary for the sustainability of the engine design.

One of the aims of the kinematic studies was to identify a suitable $r_2 : r_3$ and from the graphs above it is observed that there is some conflicting behaviour from $r_2 = 15$ precisely at the position vector analysis and when we get to the linear velocity versus angular velocity analysis, the perfect elliptical shape of the curves with $5 \leq r_2 \leq 15$ permits us to conclude a smoother ride should be expected in this range. When theoretical behaviours related to expected comportment of the system during supposed functional milestones (intake, expansion and exhaust) are included into these analysis, one will say $5 \leq r_2 \leq 20$ is the permissible design range for r_2 and for $r_3 = 50$, the ratio becomes; $0.1r_3 \leq r_2 \leq 0.4r_3$. It is worth noting that this interval falls within the design norms of the Golden Rectangle Rule.

5. Conclusion

Compressed air engine is presented in this article as a very simplified engine model. This simplicity warrants its sustainability (Rathod & Arvind, 2012) and the fact that dynamic masses have been drastically reduced, its high efficiency could be considered assured (Albritton, 1998). That notwithstanding, there is the call for another article that simulates the structural and dynamic aspects of the engine model. For sure due to the complex nature of the geometries, these simulations will have to be done with the help of more advanced simulation software.

References

Albritton, D. (1998). *What Should Be Done in a Science Assessment In Protecting the Ozone Layer: Lessons, Models, and Prospects*. ResearchGate. https://doi.org/10.1007/978-1-4615-5585-8_10

Angell, J. K., & Korshover, J. (2005). Quasi-biennial and Long-term Fluctuations in Total Ozone. *Monthly Weather Review, 101*, 426-443. https://doi.org/10.1175/1520-0493(1973)101<0426:QALFIT>2.3.CO;2

Craig, K. (2011). Fundamental Principles of Mechanical Designs. *Mechanical Design Fundamentals.*

Chau, K. T. (2014). 21 - Pure electric vehicles. In R. Folkson (Ed.), *Alternative Fuels and Advanced Vehicle Technologies for Improved Environmental Performance* (pp. 655-684). Woodhead Publishing. https://doi.org/10.1533/9780857097422.3.655

Chavda, K. (2012). Study and Development of Compressed Air Engine Single Cylinder: A Review Study. *International Journal of Advanced Engineering Technology*, 271-274.

Department of Climate Change Australia. (2008). *National Greenhouse Gas Inventory (2006).* Australian Government.

Fergusson, A. (2001). *Ozone layer Depletion and Climate Change: Understanding the linkage.* Canada: Minister

of Public Works and Government Services Canada.

Heinberg, R. (2011, July 12). Rising Cost of Fossil Fuels and the Coming Energy Crunch. *OILPRICE.COM*.

International Energy Agency. (2009). Transport, Energy and CO2. *Directorate of Sustainable Policy and Technology*.

Kahn, B. (2016, September 27). World's Atmospheric Carbon Dioxide Passes 400 PPM Threshold. Permanently. *Climate Central*.

Kavalec, C. (1999). Vehicle choice in an aging population: Some insights from a stated preference survey from California. *The Energy Journal, 20*(3), 123-138. https://doi.org/10.5547/ISSN0195-6574-EJ-Vol20-No3-5

Kronberg, N., & Shawn, W. (2019). Transport Statistics Great Britain. *Department of Transport*.

Lambert, J. (2020, August 7). Emissions Dropped during the COVID-19 pandemic. *Science News*.

Morrisette, P. M. (1995). The Evolution of Policy Responses to Stratospheric Ozone Depletion. *Natural Resources Journal, 2*.

Ngang Tangie Fru. (2019). *Zero CO2 and Zero Heat Pollution Compressed Air Engine for the Urban Transport Sector*. Yaounde Cameroon: University of Yaounde 1.

Ngang, T. F. (2019). *Zero CO2 and Zero Heat Pollution Compressed Air Engine for the Urban Transport Sector.* Yaounde Cameroon: University of Yaounde 1.

Odd Andr é, H., Arnesen, P., Torstein, A. B., & Sondell, R. S. (2020). Estimation of tank-to-wheel efficiency functions based on type approval data. *Applied Energy, 276*. https://doi.org/10.1016/j.apenergy.2020.115463

Rucks, J. W. (2015, March 17). 5 steps to an urban transportation revolution. *GreenBiz*.

Sivasakthivel, T., & Reddy, K. K. S. K. (2011). Ozone Layer Depletion and Its Effects: A Review. *International Journal of Environmental Science and Development*.

Thipse, S. (2008, Nov-Dec). Compressed air car. *TECH MONITOR*.

Thipse, S. (2008). *Compressed Air Car.* Engine Development Laboratory.

Thompson, A. (2016, September 14). August Declared Hottest on Record: NASA. *Climate Central*.

Verma, S. (2008). Air Powered Vehicle. *The Open Fuels & Energy Science Journal*, 54-56. https://doi.org/10.2174/1876973X00801010054